universe

IMPACT FACTOR 2.9

CITESCORE 3.6

Article

The Power of Relativistic Jets: A Comparative Study

Luigi Foschini, Benedetta Dalla Barba, Merja Tornikoski, Heinz Andernach, Paola Marziani, Alan P. Marscher, Svetlana G. Jorstad, Emilia Järvelä, Sonia Antón and Elena Dalla Bontà

Special Issue

Recent Advances in Gamma Ray Astrophysics and Future Perspectives

Edited by

Dr. Patrizia Romano

MDPI

https://doi.org/10.3390/universe10040156

universe

MDPI

Article

The Power of Relativistic Jets: A Comparative Study

Luigi Foschini [1,*], Benedetta Dalla Barba [1,2], Merja Tornikoski [3], Heinz Andernach [4,†], Paola Marziani [5], Alan P. Marscher [6], Svetlana G. Jorstad [6], Emilia Järvelä [7], Sonia Antón [8] and Elena Dalla Bontà [9]

1 Osservatorio Astronomico di Brera, Istituto Nazionale di Astrofisica (INAF), 23807 Merate, Italy
2 Dipartimento di Scienza e Alta Tecnologia (DiSAT), Università degli Studi dell'Insubria, 22100 Como, Italy
3 Metsähovi Radio Observatory, Aalto University, 02540 Kylmälä, Finland
4 Thüringer Landessternwarte, D-07778 Tautenburg, Germany
5 Osservatorio Astronomico di Padova, Istituto Nazionale di Astrofisica (INAF), 35122 Padova, Italy
6 Department of Astronomy, Boston University, Boston, MA 02215, USA
7 Homer L. Dodge Department of Physics and Astronomy, University of Oklahoma, Norman, OK 73019, USA
8 CFisUC, Departamento de Física, Universidade de Coimbra, 3004-516 Coimbra, Portugal
9 Dipartimento di Fisica e Astronomia, Università di Padova, 35122 Padova, Italy
* Correspondence: luigi.foschini@inaf.it
† On leave of absence from: Departamento de Astronomía, Universidad de Guanajuato, Guanajuato 36023, GTO, Mexico.

Abstract: We present the results of a comparison between different methods to estimate the power of relativistic jets from active galactic nuclei (AGN). We selected a sample of 32 objects (21 flat-spectrum radio quasars, 7 BL Lacertae objects, 2 misaligned AGN, and 2 changing-look AGN) from the very large baseline array (VLBA) observations at 43 GHz of the Boston University blazar program. We then calculated the total, radiative, and kinetic jet power from both radio and high-energy gamma-ray observations, and compared the values. We found an excellent agreement between the radiative power calculated by using the Blandford and Königl model with 37 or 43 GHz data and the values derived from the high-energy γ-ray luminosity. The agreement is still acceptable if 15 GHz data are used, although with a larger dispersion, but it improves if we use a constant fraction of the γ-ray luminosity. We found a good agreement also for the kinetic power calculated with the Blandford and Königl model with 15 GHz data and the value from the extended radio emission. We also propose some easy-to-use equations to estimate the jet power.

Keywords: relativistic jets; active galactic nuclei; Seyfert galaxies; BL Lac objects; flat-spectrum radio quasars

Citation: Foschini, L.; Dalla Barba, B.; Tornikoski, M.; Andernach, H.; Marziani, P.; Marscher, A.P.; Jorstad, S.G.; Järvelä, E.; Antón, S.; Dalla Bontà, E. The Power of Relativistic Jets: A Comparative Study. *Universe* **2024**, *10*, 156. https://doi.org/10.3390/universe10040156

Academic Editor: Ioana Dutan

Received: 16 February 2024
Revised: 25 March 2024
Accepted: 26 March 2024
Published: 27 March 2024

1. Introduction

Accreting compact objects can emit powerful relativistic jets (see [1,2] for recent reviews on jets from active galactic nuclei (AGN)). One key quantity to understand the physics of jets and its impact on the nearby environment (the host galaxy and/or the intergalactic medium) is the power—both radiative and kinetic—that is dissipated in these structures. There are many ways to estimate the power based on different observational quantities, but the results are generally not consistent, with differences of one or more orders of magnitude. Despite this clear mismatch between the various methods, very few works have been published to understand the origin of this problem.

Pjanka et al. [3] compared four methods: a one-zone leptonic model by Ghisellini et al. [4,5], radio core shifts [6,7], extended radio emission (radio lobes or steep radio spectrum) [8], and high-energy gamma-ray luminosity [5,9]. They found that the powers estimated according to the leptonic model and the radio core shifts are almost consistent, while the value derived from the γ-ray luminosity is about half, and that from the radio lobes is about one order of magnitude smaller. These calculations can be reconciled by taking into account the source variability across time (the power derived from extended radio emission is an

average over the source lifetime) or a change in the ratio between the number of leptons to hadrons (at least 15 to 1) or in the magnetization of the jet (and giving up the ideal magnetohydrodynamic theory). However, Pjanka et al. concluded that they are unable to decide which option is best.

We too made a preliminary study by comparing the interpretations of the same method by different authors [10]. Therefore, we compared the radiative power derived from the γ-ray luminosity and the Lorentz and Doppler factors from radio observations at different frequencies from [11–14]. We compared the broad-band spectral modeling by [5,15,16] and the observation of extended radio emission by [17,18]. We also compared the relationships by [19], based on the 15 GHz radio luminosity, with radiative power from the γ-ray luminosity. Although the models by Ghisellini [5] and Paliya [15,16] were described as the same (one-zone leptonic model), their results are systematically different toward low power values, with Paliya's values being about one order of magnitude greater than Ghisellini's. Something similar was found also by comparing the power calculated from the extended radio emission with differences of one to two orders of magnitudes at low powers. In this case, the reason was likely the different approaches: while Nokhrina [18] directly considered observations at 326 MHz, Meyer [17] started from 1.4 GHz observations and extrapolated to 300 MHz. The latter is not suitable for estimating the steep-spectrum radio emission from lobes because it fades as the frequency increases, and extended emission might not be detected already at GHz. The comparison of Foschini's relationship between jet power and 15 GHz radio core luminosity (see Equation (1) in [19]), with the radiative power from γ rays plus Lorentz and Doppler factors from radio observations at 43 GHz by Jorstad [11], resulted in a fair agreement, although with significant dispersion.

One major limitation of our previous work was to compare published works. Therefore, we could not select the epochs of observations, change models, or reanalyze data. In the present work, we overcome these limitations and address, in some more detail, the estimation of the jet power from a small but reliable sample of jetted AGN. Our aim is to understand the reasons of discrepancies and, if possible, to propose solutions. We also search for easy-to-use solutions, which might be of great value for the analysis of large samples of objects. A simple relationship between the power and an observed quantity or an equation linking a few observed quantities is easier to use than a detailed but complex numerical model. Obviously, the discrepancies have to be smaller than one order of magnitude to be acceptable.

We adopted the most recent value of the Hubble constant for the local Universe, $H_0 = 73.3$ km s^{-1} Mpc^{-1} from [20], and calculated the luminosity distance $d_{\rm L}$ by using the simplified equation:

$$d_{\rm L} \sim \frac{cz}{H_0}(1 + \frac{z}{2}) \ [\rm Mpc] \quad (1)$$

where c is the speed of light in vacuum and z is the redshift.

Since we are comparing different methods based on the same data, we did not consider measurement errors, which are often quite large, but we focused on the dispersion σ of the values.

2. Sample Selection

We selected the sample of the very long baseline array (VLBA) Boston University (BU) blazar program (now BEAM-ME, https://www.bu.edu/blazars/BEAM-ME.html, accessed on 27 March 2024) [11,21]. It is composed of 36 objects observed with VLBA at 43 GHz between June 2007 and January 2013. We cross-matched this sample with the catalog of revised classifications and redshifts for the jetted AGN sample in the fourth *Fermi* Large Area Telescope (LAT) catalog (4FGL) as published by [22]. We thus removed four objects: 3C 66A, S5 0716 + 71, and PKS 0735 + 17, because they have no spectroscopic redshift (only estimates from photometry or the imaging of the host galaxy), and 3C 111, because its galactic latitude is $|b| \leq 10^{\circ}$ and therefore not included in the above-cited work.

The remaining 32 objects are listed in Table 1, and were classified in [22] as follows: 21 flat-spectrum radio quasars (FSRQs), 7 BL Lac objects (BLLAC), 2 misaligned AGN (MIS, also known as radio galaxies), and 2 changing-look AGN (CLAGN). The latter type has different meanings, depending on the authors. It was originally introduced by Matt et al. [23] to indicate AGN switching from Compton-thin to Compton-thick obscuration. In more recent years, also changes in the accretion were considered (e.g., [24]). In the present case, CLAGN indicates jetted AGN with optical spectra showing dramatic changes, from a featureless continuum to a line-dominate spectrum, or vice versa, thus moving from one class to another (for example, from BLLAC to FSRQ and/or vice versa; cf. [22]). We kept in the sample both MIS and CLAGN to avoid reducing a small sample too much and to have some insight on how large viewing angles and dramatic changes in the electromagnetic emission can affect the jet power.

Table 1. Sample of jetted AGN derived from [11]. Column explanation: (1) IAU source name referred to J2000, (2) a more common alias, (3) right ascension ([deg], J2000), (4) declination ([deg], J2000), (5) classification (BLLAC: BL Lac object; MIS: misaligned AGN; FSRQ: flat-spectrum radio quasar; CLAGN: changing-look AGN), and (6) redshift. Information for columns (5) and (6) was taken from [22].

Name (1)	Alias (2)	RA (3)	Dec (4)	Class (5)	z (6)
J0238 + 1636	PKS 0235 + 164	39.66	+16.62	BLLAC	0.940
J0319 + 4130	NGC 1275	49.95	+41.51	MIS	0.0176
J0339 − 0146	PKS 0336 − 01	54.88	−1.78	FSRQ	0.852
J0423 − 0120	PKS 0420 − 01	65.82	−1.34	FSRQ	0.915
J0433 + 0521	3C 120	68.30	+5.35	MIS	0.0336
J0530 + 1331	PKS 0528 + 134	82.73	+13.53	FSRQ	2.07
J0830 + 2410	S3 0827 + 24	127.72	+24.18	FSRQ	0.941
J0831 + 0429	PKS 0829 + 046	127.95	+4.49	BLLAC	0.174
J0841 + 7053	4C +71.07	130.35	+70.89	FSRQ	2.17
J0854 + 2006	OJ 287	133.70	+20.11	BLLAC	0.306
J0958 + 6533	S4 0954 + 65	149.70	+65.56	BLLAC	0.368
J1058 + 0133	4C +01.28	164.62	+1.57	FSRQ	0.892
J1104 + 3812	Mkn 421	166.11	+38.21	BLLAC	0.0308
J1130 − 1449	PKS 1127 − 145	172.53	−14.82	FSRQ	1.19
J1159 + 2915	Ton 599	179.88	+29.24	FSRQ	0.725
J1221 + 2813	W Comae	185.38	+28.23	BLLAC	0.102
J1224 + 2122	4C +21.35	186.23	+21.38	FSRQ	0.434
J1229 + 0203	3C 273	187.28	+2.05	FSRQ	0.158
J1256 − 0547	3C 279	194.05	−5.79	FSRQ	0.536
J1310 + 3220	OP 313	197.62	+32.34	FSRQ	0.996
J1408 − 0752	PKS B1406 − 076	212.24	−7.87	FSRQ	1.49
J1512 − 0905	PKS 1510 − 089	228.21	−9.10	FSRQ	0.360
J1613 + 3412	OS 319	243.42	+34.21	FSRQ	1.40
J1626 − 2951	PKS B1622 − 297	246.52	−29.86	FSRQ	0.815
J1635 + 3808	4C +38.41	248.81	+38.13	FSRQ	1.81
J1642 + 3948	3C 345	250.74	+39.81	FSRQ	0.593
J1733 − 1304	PKS 1730 − 13	263.26	−13.08	FSRQ	0.902
J1751 + 0939	OT 081	267.89	+9.65	CLAGN	0.320
J2202 + 4216	BL Lac	330.68	+42.28	BLLAC	0.0686
J2225 − 0457	3C 446	336.45	−4.95	CLAGN	1.40
J2232 + 1143	CTA 102	338.15	+11.73	FSRQ	1.04
J2253 + 1608	3C 454.3	343.49	+16.15	FSRQ	0.858

It is worth noting that there are some slight differences in the values of the redshift with respect to [11]. Therefore, we recalculated the affected quantities (e.g., the brightness temperature) to take into account these changes. This is mostly for the sake of consistency, rather than a significant change in the affected quantities.

In addition to the Boston University blazar program, there is also another excellent VLBA program: the Monitoring of Jets in Active Galactic Nuclei with VLBA Experiments

(MOJAVE (https://www.cv.nrao.edu/MOJAVE/, accessed on 27 March 2024), [25]). We cross-matched the above-cited sample with the larger sample (447 AGN) of the MOJAVE program [26], which offers a comparable set of physical quantities measured from radio observations at 15 GHz or derived from them. All 32 objects from the BU blazar program have been observed in the MOJAVE program. Additionally, in this case, we found some cases of a slightly different redshift, and we corrected the affected quantities.

3. The Blandford and Königl Model

The first step is to use the simplified and evergreen model by Blandford and Königl [27] to estimate the jet power. For the sake of simplicity, we shortly recall the main concepts and refer to the above-cited work [27] for more details. Blandford and Königl considered a conical jet, with an opening semiangle ϕ, and the axis inclined by an angle θ with respect to the line of sight to the observer, so that the observed opening angle is $\phi_{\rm obs} = \phi/\sin\theta$. The jet is a stream of relativistic electrons with distribution:

$$N(\gamma_{\rm e}) = K\gamma_{\rm e}^{-2} \tag{2}$$

where K is a normalization constant, and $\gamma_{\rm e}$ is the random Lorentz factor of the electrons in the range $\gamma_{\rm e,min} < \gamma_{\rm e} < \gamma_{\rm e,max}$. The magnetic field B is tangled with the plasma, and the bulk motion of the electrons has a constant speed β (in units of c), linked to the measured apparent speed $\beta_{\rm app}$ via the following:

$$\beta = \frac{\beta_{\rm app}}{\beta_{\rm app}\cos\theta + \sin\theta} \tag{3}$$

The electron energy density is as follows:

$$u_{\rm e} = Km_{\rm e}c^2 \log\left(\frac{\gamma_{\rm e,max}}{\gamma_{\rm e,min}}\right) \tag{4}$$

where $m_{\rm e}$ is the electron rest mass, while the energy density of the magnetic field is as follows:

$$u_{\rm B} = \frac{B^2}{8\pi} \tag{5}$$

Equipartition between $u_{\rm e}$ and $u_{\rm B}$ is assumed via the constant $k_{\rm eq}$, generally smaller than 1 (Blandford and Königl assumed $k_{\rm eq} = 0.5$ in their example [27]).

Blandford and Königl then calculated the expected flux density at radio frequencies, given the power of the jet (Equation (29) in [27]):

$$S_\nu \sim \frac{1}{2}(1+z)k_{\rm eq}^{\frac{5}{6}}\Delta^{-\frac{17}{12}}\left(1+\frac{2}{3}k_{\rm eq}\Lambda\right)^{-\frac{17}{12}}\Gamma^{-\frac{17}{6}}\beta^{-\frac{17}{12}}\delta^{\frac{13}{6}}(\sin\theta)^{-\frac{5}{6}}\phi_{\rm obs}^{-1}P_{44}^{\frac{17}{12}}d_{\rm L,9}^{-2}\ [\rm Jy] \tag{6}$$

where S_ν is the observed flux density at the frequency ν, $\Delta = \log(r_{\rm max}/r_{\rm min})$, where $r_{\rm min}$ and $r_{\rm max}$ refer to the size of the emission region, $\Lambda = \log(\gamma_{\rm e,max}/\gamma_{\rm e,min})$; Γ is the bulk Lorentz factor; δ is the Doppler factor; $d_{\rm L,9}$ is the luminosity distance in units of Gpc; and P_{44} is the total jet power in units of 10^{44} erg s^{-1}. We can rearrange Equation (6) to calculate the jet power as a function of the observed radio flux density and the other observed physical quantities:

$$P_{44} \sim k_1 k_2 \left(\frac{S_\nu d_{\rm L,9}^2}{1+z}\right)^{12/17} \tag{7}$$

where the factor k_1 depends on the electron random Lorentz factors and the size of the emitting region:

$$k_1 = \left(\frac{1}{2}\right)^{-12/17} k_{\rm eq}^{-10/17} \Delta (1 + \frac{2}{3} k_{\rm eq} \Lambda) \tag{8}$$

while k_2 depends on the observed quantities:

$$k_2 = \Gamma^2 \beta \delta^{-26/17} (\sin\theta)^{10/17} \phi_{\rm obs}^{12/17} \tag{9}$$

The synchrotron radiative power is as follows:

$$P_{\rm rad,syn,44} \sim \frac{k_{\rm eq}}{2(1 + \frac{2}{3} k_{\rm eq} \Lambda)} P_{44} \tag{10}$$

By adopting the typical values suggested by Blandford and Königl [27] for $k_{\rm eq} = 0.5$, $\Delta = 5$, and $\Lambda = 3$, we obtain $k_1 \sim 24.5$. Therefore,

$$P_{44} \sim 24.5 k_2 \left(\frac{S_\nu d_{\rm L,9}^2}{1+z}\right)^{12/17} \tag{11}$$

$$P_{\rm rad,syn,44} \sim \frac{1}{8} P_{44} \tag{12}$$

It immediately follows that the jet kinetic power is as follows:

$$P_{\rm kin,44} \sim \frac{7}{8} P_{44}. \tag{13}$$

4. Very Long Baseline Array (VLBA) Observations

4.1. All Epochs

The data collected by the BU blazar program span from June 2007 to January 2013, while the MOJAVE program covers the years from 1994 to 2019. The first check was based on all the data available (Table 2). We noted that one object in the MOJAVE sample (J0238 + 1636) has no measurement of $\beta_{\rm app}$; therefore, we adopted the value from Jorstad et al. [11]. The MOJAVE program has also no measurement of $\phi_{\rm obs}$, and therefore, we calculated it by means of the relationship $\Gamma\phi \sim 0.1$–0.2 [3,28]. We adopted $\Gamma\phi \sim 0.11$ as suggested by [3], but tested also the case of $\Gamma\phi \sim 0.2$, resulting in no significant changes. Since we need the observed opening angle $\phi_{\rm obs}$ in Equation (6), the above-cited relationship can be rewritten as follows:

$$\phi_{\rm obs} = \frac{0.11}{\Gamma \sin\theta} \tag{14}$$

This equation was used also to calculate $\phi_{\rm obs}$ at 43 GHz for J0238 + 1636 because this measurement was missing.

We distinguished two cases. In *case 1*, the Doppler factor at 43 GHz was derived from the flux density variability of the jet knots, according to Equation (3) in [11]:

$$\delta = \frac{15.8 s d_{\rm L,9}}{\tau(1+z)} \tag{15}$$

where s is the angular size of the knot (mas), and τ is the variability time scale (years). Therefore, we corrected Equation (15) to take into account the slightly different values of z and $d_{\rm L,9}$.

Then, Γ and θ were also updated according to the well-known equations (e.g., [11,26]):

$$\Gamma = \frac{\beta_{\rm max}^2 + \delta^2 + 1}{2\beta_{\rm max}} \tag{16}$$

$$\theta = \arctan \frac{2\beta_{\rm max}}{\beta_{\rm max}^2 + \delta^2 - 1} \tag{17}$$

In *case 2*, we tested the effect of recalculating the Doppler factor at 43 GHz by using the brightness temperature ratio:

$$\delta = \frac{T_{\mathrm{b},43}}{T_{\mathrm{b,int}}} \tag{18}$$

where $T_{\mathrm{b},43}$ is the observed brightness temperature [K] (see Table 2), and $T_{\mathrm{b,int}} = 5 \times 10^{10}$ K is the theoretical intrinsic value [29]. We underline that case 1 and case 2 differ in the calculation of δ at 43 GHz (Equation (15) vs. Equation (18)). The Doppler factor at 15 GHz is always derived from the brightness temperature. It is also worth noting that we adopt β_{max} as the reference apparent speed because it correlates better with T_{b}, as suggested by [26].

Table 2. Input data corrected for different redshifts and H_0 (all epochs). Columns description: (1) source name (J2000), (2) median flux density at 15 GHz [Jy], (3) 15 GHz brightness temperature [K], (4) maximum apparent speed as measured from 15 GHz observations [*c*], (5) median flux density at 43 GHz [Jy], (6) 43 GHz brightness temperature [K], (7) maximum apparent speed as measured from 43 GHz observations [*c*], (8) Doppler factor as measured according to Equation (15), and (9) observed jet opening semiangle [deg]. Original data at 15 and 43 GHz are taken from [26] and [11], respectively. To avoid reducing the small sample too much, we considered the few cases of lower limits as detections.

Name (1)	$S_{15\,\mathrm{GHz}}$ (2)	$\log T_{\mathrm{b},15}$ (3)	$\beta_{\mathrm{max},15}$ (4)	$S_{43\,\mathrm{GHz}}$ (5)	$\log T_{\mathrm{b},43}$ (6)	$\beta_{\mathrm{max},43}$ (7)	δ_{43} (8)	ϕ_{obs} (9)
J0238 + 1636	1.33	11.70	26.27 [1]	1.77	10.97 [2]	26.27	48.75	5.84 [3]
J0319 + 4130	2.84	11.25	0.41	15.51	10.79	0.36	10.37	22.1
J0339 − 0146	1.56	12.03	24.5	1.68	11.19 [2]	31.42	14.39	7.2
J0423 − 0120	4.80	12.49	5.46	4.74	11.90	15.53	15.56	23.4
J0433 + 0521	0.958	11.36	6.28	1.67	11.46	8.7	4.33	6.6
J0530 + 1331	2.18	12.14	18.41	2.02	11.91	77.94	20.79	22.8
J0830 + 2410	1.19	11.78	19.8	1.28	11.47	18.04	21.03	24.0
J0831 + 0429	0.525	11.39	10.2	0.57	10.97	7.23	12.33	7.9
J0841 + 7053	1.50	12.14	21.51	1.73	11.20	25.15	16.80	6.8
J0854 + 2006	2.74	12.27	15.14	4.68	11.88	8.6	7.9	33.0
J0958 + 6533	0.903	11.76	14.8	1.05	11.45	17.58	7.78	21.0
J1058 + 0133	3.57	12.50	6.61	4.02	11.61	14.14	18.42	24.8
J1104 + 3812	0.319	11.14	0.218	0.28	10.18	1.07	23.42	55.2
J1130 − 1449	1.12	11.80	19.8	1.76	11.36	23.37	19.68	15.4
J1159 + 2914	1.57	11.95	24.6	1.40	11.59	15.47	10.75	13.6
J1221 + 2813	0.226	11.31	8.2	0.25	10.79	4.76	8.96	9.2
J1224 + 2122	1.40	11.83	21.8	1.19	11.66	13.81	6.72	16.2
J1229 + 0203	3.52	11.95	14.91	11.88	12.51	11.83	3.97	6.6
J1256 − 0547	11.94	12.76	20.5	18.05	11.92	16.01	16.54	47.4
J1310 + 3220	1.55	11.99	27.5	2.14	10.95	13.73	19.37	58.4
J1408 − 0752	0.802	12.06	22.77	0.59	11.32	29.42	10.89	16.4
J1512 − 0905	1.87	11.95	28.0	2.44	11.15	29.6	31.98	11.4
J1613 + 3412	2.73	12.25	31.1	1.53	11.09	9.82	7.29	20.8
J1626 − 2951	0.959	12.01	12.0	1.35	11.34	11.04	8.68	30.8
J1635 + 3808	2.02	12.46	30.8	2.93	11.86	10.17	12.71	41.2
J1642 + 3948	3.27	12.29	19.37	4.47	11.63	19.45	10.77	18.6
J1733 − 1304	3.07	12.29	27.3	3.31	11.92	23.52	7.27	16.2
J1751 + 0939	3.52	12.62	6.85	3.60	11.65	17.66	15.97	26.2
J2202 + 4216	2.28	11.87	10.0	4.21	11.99 [2]	11.89	7.00	6.0
J2225 − 0457	4.75	12.30	17.7	3.82	11.62	22.20	13.19	22.0
J2232 + 1143	2.04	12.38	20.0	2.71	11.59	27.93	28.49	23.8
J2253 + 1608	3.53	12.26	17.0	14.44	12.22	9.06	22.35	22.6

[1] Missing. Value from 43 GHz measurements. [2] Lower limit. [3] Missing. Value from Equation (14).

Figure 1 shows the comparison of δ as measured with the two cited methods. We noted some cases with extreme differences: J0238 + 1636, $\delta_1 \sim 49$, $\delta_2 \sim 2$; J1104 + 3812, $\delta_1 \sim 23$, $\delta_2 \sim 0.30$; J1229 + 0203, $\delta_1 \sim 4$, $\delta_2 \sim 65$. The reasons might be that, e.g., J0238 + 1636 has no measured $\phi_{\rm obs}$, and its $T_{\rm b,43}$ is a lower limit, and J1229 + 0203 has the highest $T_{\rm b,43}$. This might imply the breakdown of the equipartition assumption for the observed brightness temperature $T_{\rm b,obs} > 10^{13}$ K, as already noted in [11,29]. The case of J1104 + 3812 might be due to the so-called Doppler crisis in BL Lacs [30,31].

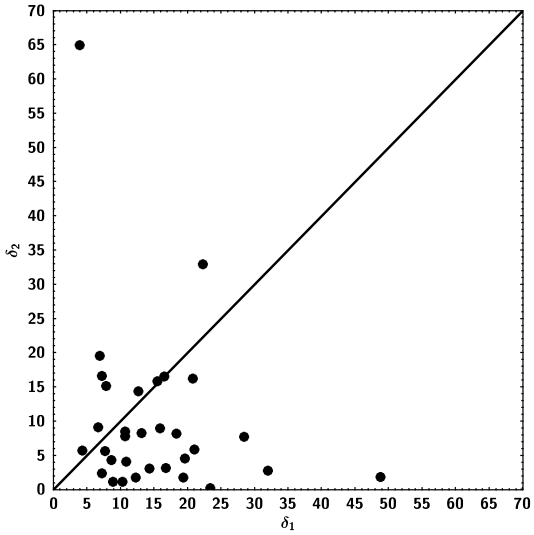

Figure 1. Doppler factor δ_1 (case 1) estimated from 43 GHz data and Equation (15) with the cosmology adopted in the present work vs. δ_2 (case 2) calculated from the brightness temperature. The continuous line indicates the equality of the two values.

Figure 2 displays the total jet power in the two cases and compared with the values derived from 15 GHz data. It is also worth studying the distribution of the coefficients k_2 (see Equation (9)), which is shown in Figure 3 for case 1.

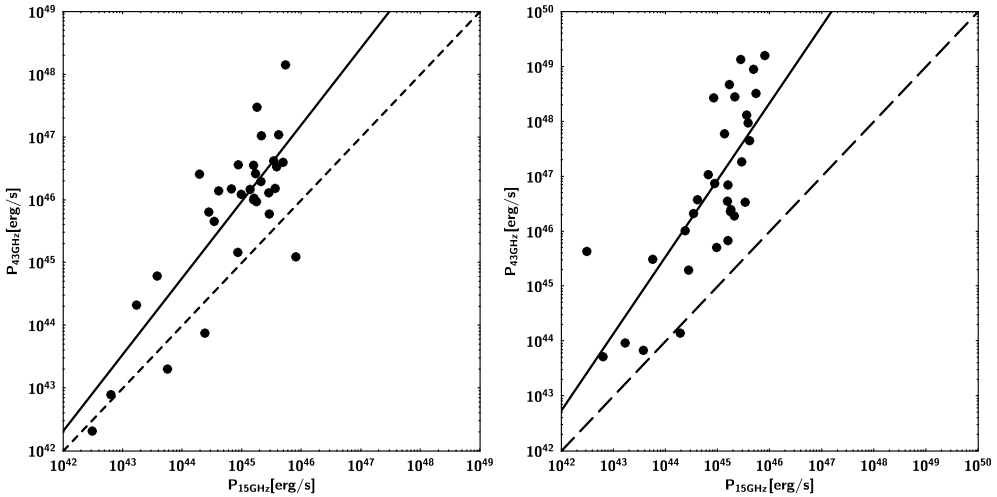

Figure 2. Total jet power calculated from Equation (11) and all the data from 15 and 43 GHz observations: (**left panel**) case 1; (**right panel**) case 2. The dashed line represents the equality of the two powers, while the continuous line is the linear fit to the data.

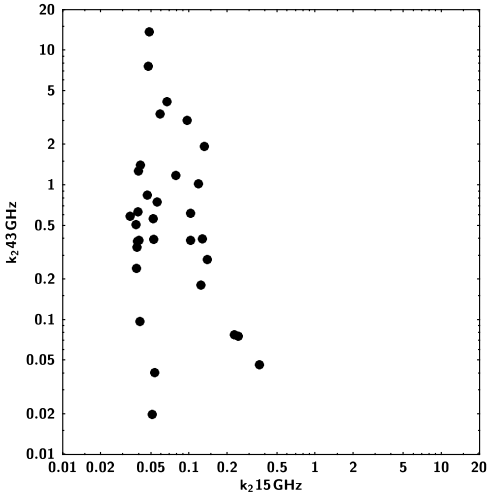

Figure 3. Distribution of k_2 values at 15 and 43 GHz for case 1.

The mean value of k_2 is 0.088 ($\sigma \sim 0.072$), and 1.4 ($\sigma \sim 2.6$) for 15 and 43 GHz, respectively (please note that $k_2 > 0$ by definition, so the dispersion is mostly toward values greater than the average). In case 2 (not shown), the dispersion increases to ∼131, while the mean value rises to ∼61. It is worth noting that the distribution of k_2 for 15 GHz data is quite narrow, with all the values between ∼0.034 and ∼0.36.

It is evident that the derivation of the Doppler factor from the brightness temperature at 43 GHz (case 2) leads to a more pronounced divergence at higher powers and a larger dispersion. The linear fit in the following form:

$$\log P_{43\,\mathrm{GHz}} = m \log P_{15\,\mathrm{GHz}} + C \tag{19}$$

gives the following values: $m \sim 1.22$ and $C \sim -8.9$ for case 1; $m \sim 1.40$ and $C \sim -16$ for case 2. The correlation factor ρ is 0.82 and 0.77 for case 1 and case 2, respectively, while the dispersion σ is 0.72 and 0.96.

Nonetheless, the relatively small range of k_2 values (particularly at 15 GHz, see Figure 3) offers an interesting possibility to derive the jet power only on the basis of the flux density at radio frequencies, although some caveats must be taken into account (see Section 8).

4.2. Overlapping Epochs

We remind the reader that 43 GHz data span from June 2007 to January 2013 [11], while 15 GHz data cover the years from 1994 to 2019 [26]. In the previous subsection, we considered all the available epochs, but now we want to study the case of overlapping epochs. Therefore, we collected 15 GHz data only if observed between 1 June 2007, and 31 January 2013 (Table 3). The results are shown in Figure 4.

There are no significant changes with respect to the previous cases. The linear fit gives these parameters: $m \sim 1.26$, $C \sim -11$, $\rho \sim 0.82$, $\sigma \sim 0.71$. However, we note an increase in the mean value of k_2 at 15 GHz and its dispersion, from ∼0.088 ($\sigma \sim 0.072$) to ∼0.18 ($\sigma \sim 0.26$). Since k_2 is a function of β, Γ, δ, θ, and ϕ_{obs} (see Equation (9)), a change in the observing epochs results in a different median $T_{\mathrm{b,15\,GHz}}$, which in turn affects δ and all the other parameters of k_2. The possibility of having a greater or smaller mean value and dispersion depends on the activity of the objects during the selected time interval. Anyway, in the present case, the distribution is still narrow, with only two values greater than the previous limit of ∼0.36. The two objects are J0831 + 0429 ($k_2 \sim 0.57$) and J1221 + 2813 ($k_2 \sim 1.5$). Given the lack of significant changes with respect to $P_{43\,\mathrm{GHz}}$, we concluded that changes in k_2 were partially compensated by changes in flux density.

Table 3. Input data corrected for different redshifts and H_0 (overlapping epochs, from June 2007 to January 2013). Columns description: (1) source name (J2000), (2) median flux density at 15 GHz [Jy], (3) 15 GHz brightness temperature [K], and (4) median flux density at 37 GHz [Jy]. Original data at 15 GHz from [26]. See Section 5 for 37 GHz data of the Metsähovi Radio Observatory.

Name (1)	$S_{15\,\mathrm{GHz}}$ (2)	$\log T_{b,15}$ (3)	$S_{37\,\mathrm{GHz}}$ (4)
J0238 + 1636	3.37	12.31	1.50
J0319 + 4130	3.26	11.27	17.34
J0339 − 0146	1.58	12.09	2.33
J0423 − 0120	4.65	12.27	5.18
J0433 + 0521	0.675	11.22	1.95
J0530 + 1331	1.69	12.26	1.69
J0830 + 2410	1.23	11.74	1.42
J0831 + 0429	0.434	11.32	0.724
J0841 + 7053	2.10	12.56	2.20
J0854 + 2006	3.99	12.27	5.01
J0958 + 6533	1.07	11.72	1.19
J1058 + 0133	4.37	12.56	4.25
J1104 + 3812	0.292	11.12	0.428
J1130 − 1449	1.32	11.94	–
J1159 + 2914	1.53	11.79	1.61
J1221 + 2813	0.216	11.06	0.363
J1224 + 2122	1.68	12.21	1.69
J1229 + 0203	3.66	11.86	16.49
J1256 − 0547	9.82	12.72	18.67
J1310 + 3220	2.44	12.09	2.20
J1408 − 0752	0.708	11.75	0.812
J1512 − 0905	2.38	12.00	2.62
J1613 + 3412	1.61	12.07	2.35
J1626 − 2951	0.959	12.02	–
J1635 + 3808	2.27	12.26	3.62
J1642 + 3948	4.86	12.37	5.69
J1733 − 1304	3.32	12.30	3.69
J1751 + 0939	4.70	12.72	3.38
J2202 + 4216	3.44	11.98	4.50
J2225 − 0457	4.56	11.89	3.43
J2232 + 1143	2.11	12.46	2.79
J2253 + 1608	9.16	12.76	7.21

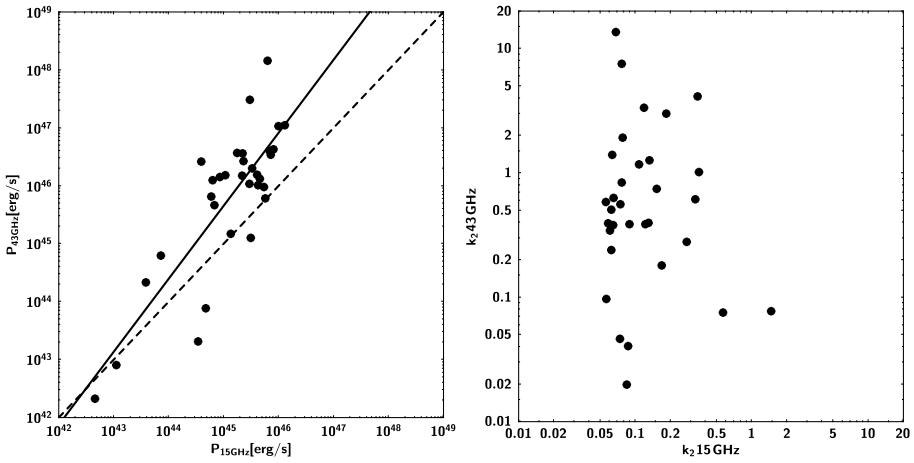

Figure 4. (**Left panel**) Total jet power calculated with Equation (11) and overlapping epoch data from 15 and 43 GHz observations. The dashed line represents the equality of the two powers, while the continuous line is the linear fit to the data. (**Right panel**) Distribution of k_2 values at 15 and 43 GHz.

5. Single-Dish Observations

The next test is to use the above calculated k_2 factors to estimate the jet power from single-dish observations. This type of observations does not allow for measuring or deriving all the quantities necessary to calculate k_2 (which are $\delta, \Gamma, \beta, \theta, \phi_{\rm obs}$, cf. Equation (9)): it is possible to measure only δ from the brightness temperature [13,32], but then it is necessary to take $\beta_{\rm app}$ from VLBA observations to derive the other quantities according to Equations (14), (16), and (17). Therefore, we can try to use k_2 as measured from the above-cited VLBA observations coupled to the flux density as measured from single-dish observations.

Data from the Metsähovi Radio Observatory (https://www.metsahovi.fi/opendata/, accessed on 27 March 2024) (MRO) of Aalto University (Finland) were used. MRO is a $\sim$14 m single dish equipped with a 1 GHz-band dual-beam receiver centered at 36.8 GHz. The high electron mobility pseudomorphic transistor (HEMPT) front end operates at ambient temperature. The observations, with typical exposures of $\sim 10^3$ s, are Dicke-switched ON–ON observations, alternating between the source and the sky in each feed horn. The detection threshold is $\sim$0.2 Jy in the best case. Calibration sources were the HII regions DR 21, NGC 7027, 3C 274, and 3C 84. More information about data reduction and analysis can be found in [33].

All the objects in Table 1 were monitored for more than 30 years, with the exception of J1130 − 1449 and J1626 − 2951. For the sake of simplicity, we considered only the case of overlapping epochs (see Table 3).

The results are displayed in Figure 5. We note a very good correlation between the new values of jet power from MRO at 37 GHz and the values of MOJAVE (15 GHz) and BU (43 GHz), with a best result if k_2 is measured from VLBA observations at the closer frequency (43 GHz), as expected. The linear fit (cf. Equation (19)) gives the following results:

- k_2 from MOJAVE (15 GHz): $m \sim 1.08$, $C \sim -3.8$, $\rho \sim 0.99$, $\sigma \sim 0.14$;
- k_2 from BU (43 GHz): $m \sim 1.00$, $C \sim -0.46$, $\rho \sim 1.00$, $\sigma \sim 0.067$;

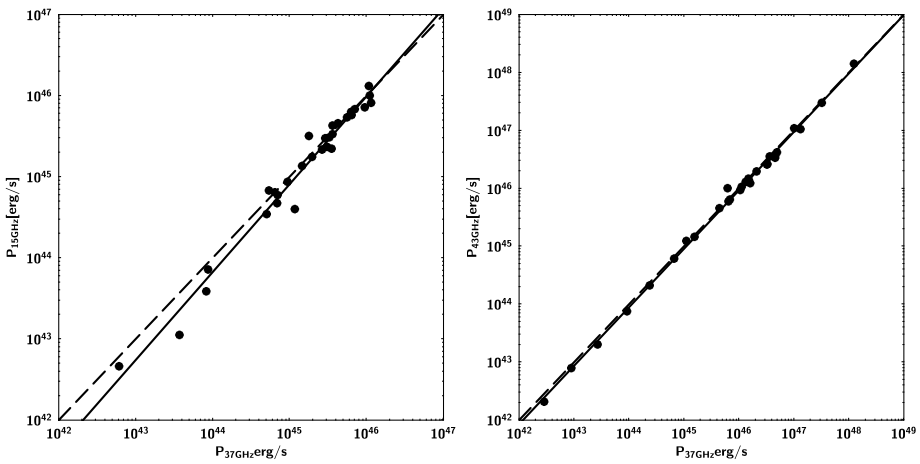

Figure 5. (**Left panel**) Total jet power derived from 37 GHz flux density and k_2 from 15 GHz observations vs. jet power from the same observations. (**Right panel**) Total jet power calculated by using 37 GHz flux density and k_2 from 43 GHz observations vs. jet power from the same observations. The dashed line represents the equality of the two powers, while the continuous line is the linear fit to the data.

6. Kinetic Power Estimated from the Extended Emission

The extended radio emission offers the opportunity to estimate the kinetic power of the jet. McNamara et al. [34] found a deficit of X-ray emission from the surrounding cluster at the location of the radio lobes of Hydra A, indicating that the jet had excavated cavities in the intergalactic medium. Then, by studying these X-ray cavities of a sample of radio

galaxies in clusters, Bîrzan et al. [35] found a correlation between the jet kinetic power and its extended radio emission at 327 MHz:

$$\log \frac{P_{\rm kin}}{10^{42}} = 0.51 \log \frac{P_{327\,\rm MHz}}{10^{40}} + 1.51 \quad (20)$$

where $P_{\rm kin}$ is the jet kinetic power [erg/s], while $P_{327\,\rm MHz}$ is the radio power as measured at 327 MHz [erg/s]. Later, Cavagnolo et al. [36] enlarged the sample by adding also isolated giant elliptical galaxies, and proposed a new relationship based on the extended radio emission measured at 200–400 MHz:

$$\log \frac{P_{\rm kin}}{10^{42}} = 0.64 \log \frac{P_{200-400\,\rm MHz}}{10^{40}} + 1.54 \quad (21)$$

where $P_{200-400\,\rm MHz}$ is the radio power as measured at 200–400 MHz [erg/s]. The authors also proposed a relationship with the radio power as measured at 1.4 GHz, but this is less reliable [10,35,36], and therefore, we do not consider it.

To measure the radio power, we followed the procedure outlined in [36], and extracted the radio data from the CATS database (https://www.sao.ru/cats/, accessed on 27 March 2024) [37]. As noted by Cavagnolo [36], it is difficult to find 327 MHz data for all the objects, and therefore, the search was extended to the range 200–400 MHz. In the case of our sample, we found 327 MHz data for 21/32 objects. To avoid reducing our small sample too much, we used radio data at close frequencies (227, 318, 325, 333 MHz) when 327 MHz data were not available. In the case of 200–400 MHz, we also considered the cited frequency range with a tolerance of ±10%. We performed the K-correction of the radio fluxes by adopting an average spectral index $\alpha = 0.8$ ($S_\nu \propto \nu^{-\alpha}$), as performed by [36]. We did not restrict the selected data from observations in the period 2007–2013 because the time necessary to excavate cavities in the intergalactic medium is of the order of several 10^8 years (e.g., [34]). Therefore, the measure of the kinetic power refers to an average over a very long time scale. The flux densities are displayed in Table 4.

Figure 6 shows comparisons of the jet kinetic power as calculated with Equations (20) and (21). The two values are well correlated ($\rho \sim 0.99$, $\sigma \sim 0.084$), but there is an evident divergence at high radio powers ($m \sim 1.24$, $C \sim -10.6$). This is somehow expected, given the different slopes of the two relationships ($0.64/0.51 \sim 1.25$, cf. Equations (20) and (21)). The reason for this divergence might be the different samples adopted by Bîrzan [35] and Cavagnolo [36]: while the former built the correlation by selecting a sample of radio galaxies in clusters (where, given the density and temperature of the intergalactic gas, it is easier to detect X-ray cavities), the latter added also a group of isolated giant elliptical galaxies (where X-ray cavities might be more difficult to detect).

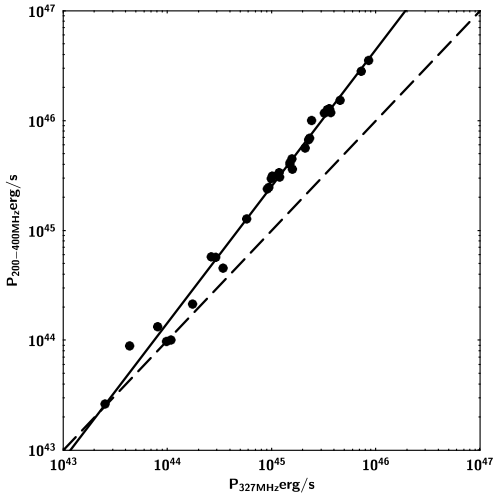

Figure 6. Comparison of the jet kinetic power as estimated from Equations (20) and (21). The dashed line represents the equality of the two powers, while the continuous line is the linear fit to the data.

Table 4. Input data for the kinetic power. Column description: (1) source name (J2000), (2) median flux density at 327 MHz [Jy], and (3) median flux density at 200–400 MHz [Jy]. All the data were extracted from the CATS database [37].

Name (1)	$S_{327\,\mathrm{MHz}}$ (2)	$S_{200-400\,\mathrm{MHz}}$ (3)
J0238 + 1636	1.04	1.26
J0319 + 4130	42.8 [1]	27.06
J0339 − 0146	0.943	1.33
J0423 − 0120	0.820	1.20
J0433 + 0521	2.37	6.33
J0530 + 1331	1.13 [1]	1.05
J0830 + 2410	0.660 [2]	0.770
J0831 + 0429	1.19 [2]	0.837
J0841 + 7053	5.07	5.07
J0854 + 2006	0.790	1.15
J0958 + 6533	0.624 [1]	0.742
J1058 + 0133	4.39	4.42
J1104 + 3812	0.961	1.14
J1130 − 1449	4.51 [3]	5.35
J1159 + 2914	3.52	2.71
J1221 + 2813	1.45	0.790
J1224 + 2122	3.98 [2]	4.80
J1229 + 0203	62.89	64.0
J1256 − 0547	14.79	14.58
J1310 + 3220	1.43	1.42
J1408 − 0752	0.535 [4]	0.584
J1512 − 0905	2.51	2.73
J1613 + 3412	2.55	3.11
J1626 − 2951	2.37 [4]	2.46
J1635 + 3808	2.51	2.31
J1642 + 3948	9.93	8.70
J1733 − 1304	4.66	7.61
J1751 + 0939	1.17 [2]	0.720
J2202 + 4216	1.82 [1]	2.77
J2225 − 0457	12.71	12.15
J2232 + 1143	6.99	7.88
J2253 + 1608	11.67	12.44

[1] From 325 MHz observations. [2] From 318 MHz observations. [3] From 333 MHz observations. [4] From 227 MHz observations.

Figure 7 displays the four comparisons between the kinetic power calculated with Equation (13) and data from 15 or 43 GHz observations and the values calculated with Equation (20) or Equation (21) with the measurements of the extended radio emission at MHz frequencies.

The linear fits give these values:

- 327 MHz vs. 15 GHz: $m \sim 1.14$, $C \sim -6.2$, $\rho \sim 0.89$, $\sigma \sim 0.37$;
- 327 MHz vs. 43 GHz: $m \sim 1.65$, $C \sim -28$, $\rho \sim 0.84$, $\sigma \sim 0.68$;
- 200–400 MHz vs. 15 GHz: $m \sim 0.91$, $C \sim 3.9$, $\rho \sim 0.89$, $\sigma \sim 0.38$;
- 200–400 MHz vs. 43 GHz: $m \sim 1.35$, $C \sim -15.5$, $\rho \sim 0.86$, $\sigma \sim 0.64$.

All the powers are well correlated ($\rho \sim 0.84$–0.89), showing a smaller dispersion when using 15 GHz data. In all cases, we noted a systematic underestimation of the power as calculated with Equation (13) for weak sources, with $P_{\mathrm{kin}} \lesssim 10^{44}$ erg/s (or an overestimation of the relationships based on the extended radio emission). The comparison with 43 GHz data shows a clear divergence toward higher radio powers. One source of bias is the fact that we used the integrated flux density, while we should have taken only the steep spectrum emission of the lobes. However, since our sources have a moderate to high redshift (with a few exceptions), it is not possible to disentangle the core from the lobes.

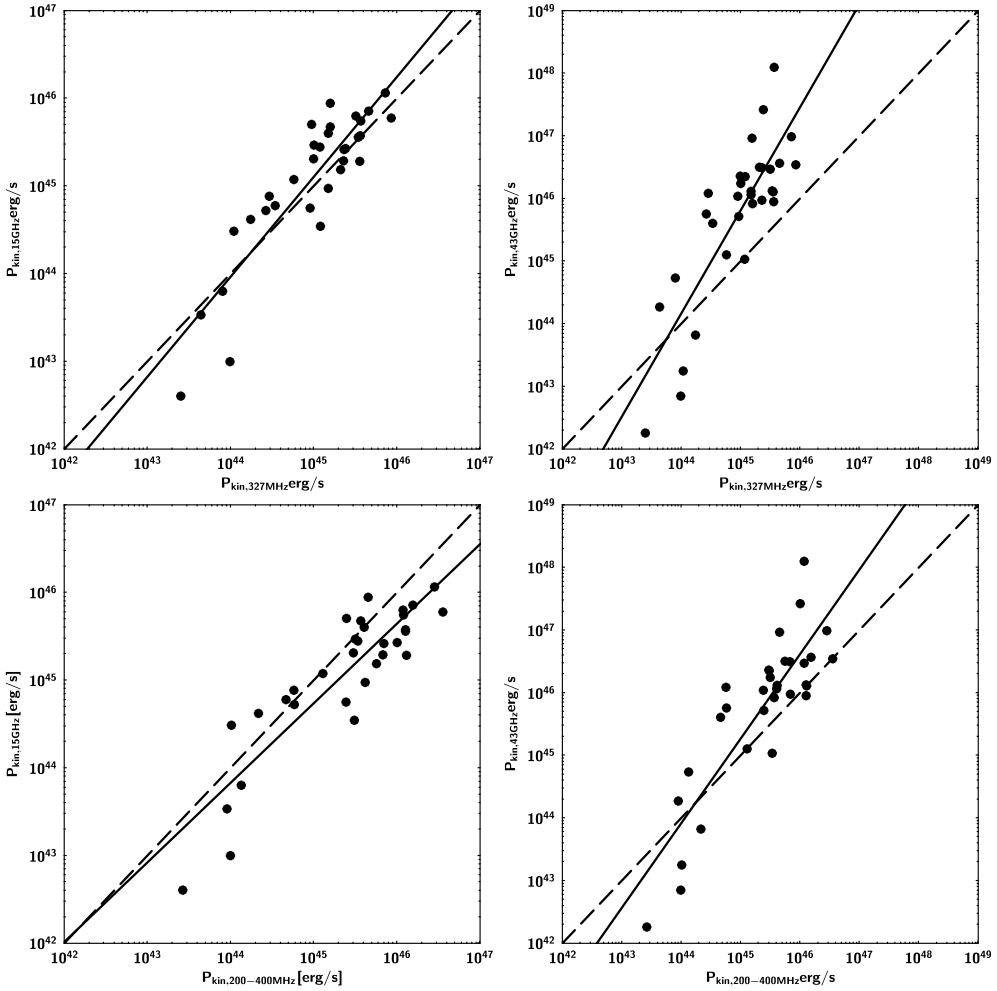

Figure 7. Kinetic jet power. (**Upper panels**) Comparison of Equations (13) and (20) with 15 GHz data (**left**) and 43 GHz data (**right**). (**Lower panels**) Comparison of Equations (13) and (21) with 15 GHz data (**left**) and 43 GHz data (**right**). The dashed line represents the equality of the two powers, while the continuous line is the linear fit to the data.

We would also like to note that Equations (20) and (21) are not the result of a theoretical calculation, but are correlations derived from observed quantities. Therefore, as is well known that correlation is not causation, the above-cited relationships heavily rely on the adopted samples, as also shown by the change in the slope from Equation (20) to Equation (21) displayed in Figure 6.

7. Radiative Power

The last test is with the radiative power as measured at high-energy γ rays by the *Fermi* Large Area Telescope (LAT) [38]. Since all the versions of the LAT catalogs cover a time span greater than the Boston University program [11], we extracted the data from the *Fermi* LAT Light Curve Repository (https://fermi.gsfc.nasa.gov/ssc/data/access/lat/LightCurveRepository/index.html, accessed on 27 March 2024) [39] covering only the epoch of the Boston University program (2007–2013). This web site is an automatic generator of light curves based on the likelihood with a power-law model and with a limited selection of parameters. We selected a 1-month time bin and left the photon index free to vary. We extracted the light curves starting from the beginning of LAT operations (August 2008) until January 2013, and then calculated the weighted mean of the observed 0.1–100 GeV flux F_γ and the spectral index α_γ (Table 5).

Table 5. *Fermi*/LAT data in the period August 2008–January 2013. Column description: (1) source name (J2000), (2) $0.1 - 100$ GeV flux [10^{-11} erg cm^{-2} s^{-1}], and (3) spectral index α_γ. All the data were downloaded from the *Fermi* LAT Light Curve Repository [39].

Name (1)	$F_{0.1-100\,\mathrm{GeV}}$ (2)	α_γ (3)
J0238 + 1636	10.0	1.20
J0319 + 4130	22.0	1.07
J0339 − 0146	4.6	1.50
J0423 − 0120	5.5	1.40
J0433 + 0521	1.5	1.70
J0530 + 1331	3.5	1.60
J0830 + 2410	3.2	1.70
J0831 + 0429	4.0	1.20
J0841 + 7053	3.4	1.80
J0854 + 2006	6.4	1.20
J0958 + 6533	1.6	1.40
J1058 + 0133	8.2	1.20
J1104 + 3812	44.0	0.73
J1130 − 1449	2.1	1.60
J1159 + 2914	8.2	1.30
J1221 + 2813	4.0	1.20
J1224 + 2122	30.0	1.60
J1229 + 0203	18.0	2.00
J1256 − 0547	23.0	1.40
J1310 + 3220	2.8	1.50
J1408 − 0752	2.1	1.40
J1512 − 0905	52.0	1.46
J1613 + 3412	1.3	1.40
J1626 − 2951	2.7	1.70
J1635 + 3808	20.0	1.40
J1642 + 3948	4.6	1.20
J1733 − 1304	6.0	1.50
J1751 + 0939	4.4	1.30
J2202 + 4216	17.0	1.28
J2225 − 0457	2.1	1.60
J2232 + 1143	14.0	1.50
J2253 + 1608	174	1.50

From these values, we calculated the 0.1–100 GeV luminosity:

$$L_\gamma = 4\pi d_\mathrm{L}^2 \frac{F_\gamma}{(1+z)^{1-\alpha_\gamma}} \tag{22}$$

The minimum radiative power $P_{\mathrm{rad},\gamma}$ from high-energy γ rays (i.e., via inverse-Compton scattering) can be estimated as follows [40]:

$$P_{\mathrm{rad},\gamma} \sim \frac{\Gamma^2}{\delta^4} L_\gamma \tag{23}$$

The values of Γ and δ can be taken from the VLBA observations at 15 and 43 GHz. Then, $P_{\mathrm{rad},\gamma}$ can be compared with the synchrotron radiative power calculated according to Equation (12). The results are displayed in Figure 8.

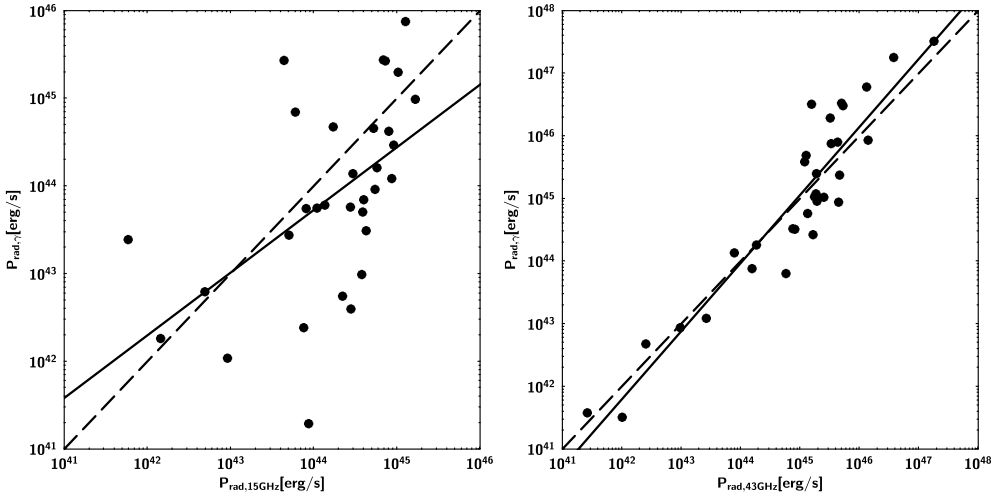

Figure 8. Radiative jet power. Comparison of values from high-energy γ rays and radio observations at 15 GHz (**left panel**) and at 43 GHz (**right panel**). The dashed line represents the equality of the two powers, while the continuous line is the linear fit to the data.

We note a good agreement, with a smaller dispersion when using 43 GHz data. The results of the linear fits are as follows:

- γ rays vs. 15 GHz: $m \sim 0.71$, $C \sim 12$, $\rho \sim 0.54$, $\sigma \sim 0.92$;
- γ rays vs. 43 GHz: $m \sim 1.09$, $C \sim -3.9$, $\rho \sim 0.94$, $\sigma \sim 0.51$.

It is worth noting that Equation (12) calculates the radiative power emitted via the synchrotron process, while the radiative power measured at high-energy γ rays can have a significant contribution from the external Compton process in FSRQs. It is known (e.g., [41]) that the total power radiated by relativistic electrons is as follows:

$$P_{\rm rad,tot} = P_{\rm rad,syn} + P_{{\rm rad},\gamma} = \frac{4}{3}\sigma_{\rm Th} c \gamma_e^2 u_{\rm B}(1 + k_{CD}) \tag{24}$$

where $P_{\rm rad,syn}$ is the power dissipated via synchrotron radiation, $P_{{\rm rad},\gamma}$ is the power due to the inverse-Compton process, and $\sigma_{\rm Th} \sim 0.66 \times 10^{-28}$ m^2 is the Thompson cross section. The Compton dominance parameter $k_{\rm CD}$ is defined as follows:

$$k_{\rm CD} = \frac{u_{\rm seed}}{u_{\rm B}} \tag{25}$$

where $u_{\rm seed}$ is the energy density of the seed photon field (from accretion disk, broad-line region, molecular torus, etc.). The Compton dominance can be measured from the observations of the peaks of synchrotron and inverse-Compton emissions:

$$k_{\rm CD} \sim \frac{\nu F_\nu^{\rm IC}}{\nu F_\nu^{\rm syn}} \tag{26}$$

From the inspection of a large sample of spectral energy distributions (SEDs) of blazars (e.g., [42]), it is possible to estimate $k_{\rm CD} \sim 1$ for BL Lac objects and $k_{\rm CD} \sim 10$ for FSRQs. Therefore, we applied this correction to FSRQs, and the results are displayed in Figure 9.

The comparison of the powers from 43 GHz and $\gamma-$ray observations does not change, with the linear fit giving these values: $m \sim 0.85$, $C \sim 6.3$, $\rho \sim 0.93$, $\sigma \sim 0.51$. However, the comparison with 15 GHz data is not so good: $m \sim 0.47$, $C \sim 22$, $\rho \sim 0.51$, $\sigma \sim 0.94$).

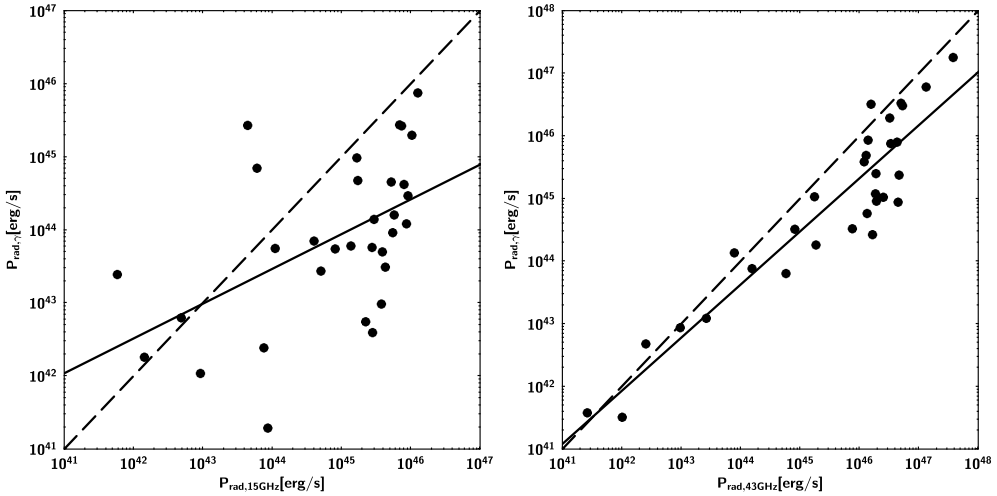

Figure 9. Radiative jet power corrected for the Compton dominance. Comparison of values from high-energy γ rays and radio observations at 15 GHz (**left panel**) and at 43 GHz (**right panel**). The dashed line represents the equality of the two powers, while the continuous line is the linear fit to the data.

The reason seems to be the use of the brightness temperature to estimate the Doppler factor, as shown already in Section 4. As a matter of fact, if we adopt the same method also for 43 GHz data, the consistency with the radiative power from γ-ray observations is lost (Figure 10). The linear fit is still acceptable, but with a large dispersion: $m \sim 1.10$, $C \sim -4.5$, $\rho \sim 0.83$, and $\sigma \sim 1.29$. Another source of bias is the use of a single value of $k_{\rm CD}$ for all FSRQs. This quantity depends on the characteristics of the source and its activity (an outburst can result in a greater value of $k_{\rm CD}$).

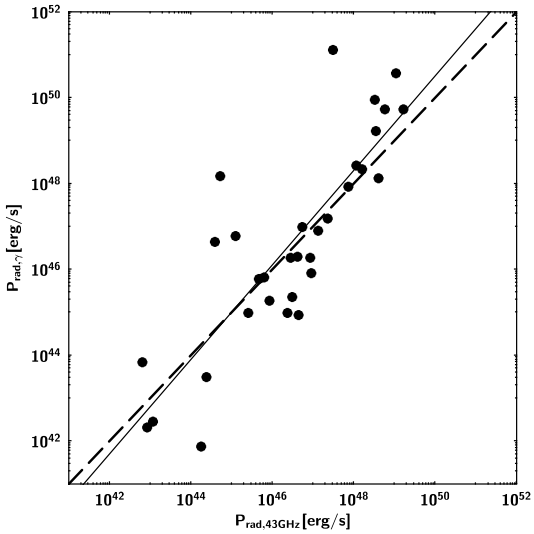

Figure 10. Radiative jet power corrected for the Compton dominance. Comparison of values from high-energy γ rays and radio observations at 43 GHz, with the Doppler factor calculated by using the brightness temperature (case 2, Section 4). The dashed line represents the equality of the two powers, while the continuous line is the linear fit to the data.

8. Fudge Factors

As noted in Section 4, the value of k_2 (see Equation (9)) is within a small range, particularly for 15 GHz data, with some exceptions. Therefore, we can try estimating the jet power by setting k_2 equal to a constant value (mean, median, etc.). We selected $k_2 = 0.183$, which is the median value calculated by selecting all the available epochs. Therefore, Equation (11) becomes the following:

$$P_{44} \sim 4.5 \left(\frac{S_\nu d_{\mathrm{L},9}^2}{1+z} \right)^{12/17} \tag{27}$$

We then consider as reference the total jet power at 43 GHz, calculated with Equation (11), and compare it with the power at 15 and 37 GHz calculated with Equation (27). The only variable is now the flux density at the selected frequency (15 or 37 GHz). The results are shown in Figure 11.

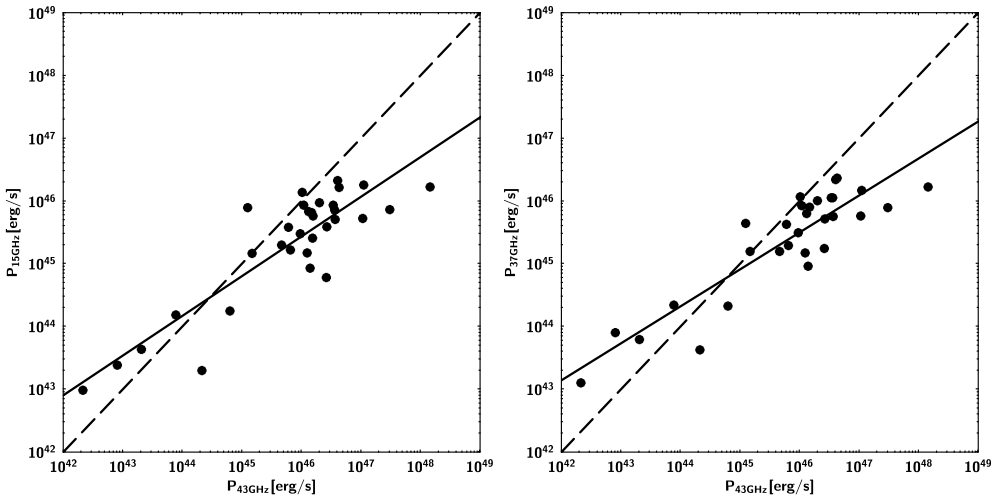

Figure 11. Total jet power calculated with a constant k_2 (Equation (27)) and flux densities at 15 (**left panel**) and 37 GHz (**right panel**) compared with the power at 43 GHz. The dashed line represents the equality of the two powers, while the continuous line is the linear fit to the data.

The linear fit gives the following results:

- 43 vs. 15 GHz: $m \sim 0.63$, $C \sim 16$, $\rho \sim 0.87$, $\sigma \sim 0.44$;
- 43 vs. 37 GHz: $m \sim 0.59$, $C \sim 18$, $\rho \sim 0.89$, $\sigma \sim 0.38$,

with slightly better values for 37 GHz, as expected. However, the slope ∼0.6 indicates a divergence toward low and high powers. We note that selecting another value for k_2 (median or average from another data set) will change only the value of C, but not all the others. The dispersion is contained within ∼0.4.

We also studied the distributions of the correction factor Γ^2/δ^4 to be applied to the γ-ray luminosity to estimate the radiative power (cf. Equation (23)). We adopted the median calculated from all data, which is $\Gamma^2/\delta^4 \sim 0.0027$. We adopted the latter value as constant in Equation (23) and compared the radiative power estimated with the proper value for each source (Figure 12).

The result of the linear fit is now as follows:

- γ vs. 15 GHz: $m \sim 0.97$, $C \sim 0.43$, $\rho \sim 0.90$, $\sigma \sim 0.56$;
- γ vs. 43 GHz: $m \sim 0.64$, $C \sim 15$, $\rho \sim 0.81$, $\sigma \sim 0.75$.

This time, there is a better agreement with 15 GHz data, but it is worth reminding that a good correlation does not imply a causation. This agreement is likely to be a chance coincidence because the previous tests (see Section 7, Figure 8, left panel, and Figure 9, left panel) do not display any hint of such agreement ($\rho \sim 0.51$–0.54). The only suitable explanation is that, by using constant fudge factors, most of fluctuations have been smoothed out by a mere chance coincidence. Taking constant average values for k_2 and Γ^2/δ^4 has no physical reason and is only for our convenience to get rid of the lack of adequate measurements.

The comparison with the radiative power estimated from 43 GHz data is still acceptable, but with a larger dispersion and a divergence at high powers.

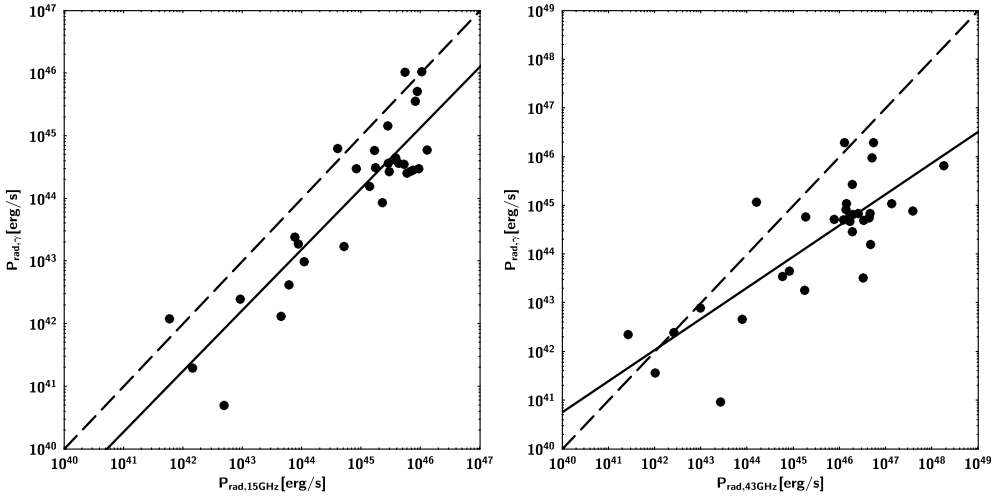

Figure 12. Radiative jet power calculated with a constant Γ^2/δ^4 compared with the power estimated with Γ^2/δ^4 from 15 GHz (**left panel**) and 43 GHz data (**right panel**). The dashed line represents the equality of the two powers, while the continuous line is the linear fit to the data.

9. Discussion and Conclusions

We compared the jet power as measured by different methods mostly based on radio observations. We can summarize the main results as follows:

- The jet power estimates based on the Blandford and Königl model [27] plus VLBA data at 15 and 43 GHz are in good agreement (Section 4). The almost simultaneity of observations does not imply significant changes in the calculated jet power, at least with the present data set (Section 4.2). One source of bias is the measurement of the Doppler factor δ via the brightness temperature (see Equation (18) and Figure 1). This problem has already been noted by several authors (e.g., [11,13,43], and particularly see the extensive discussion in [26]), and is related to both the physics of the jets (opacity, absorption, activity of the jet, etc.) and the instrumental/observational issues (frequency, cadence of observations, etc.). We do not know the intrinsic brightness temperature for any source and cannot measure it. Therefore, we need either to make theoretical hypotheses [29] or to follow a statistical approach by assuming that every jetted AGN has more or less the same T_b equal to the median or the mean of the sample [26]. The approach proposed by Jorstad et al. [11,43] to calculate δ (cf. Equation (15)) based on the flux variability is much more reliable, as shown by the excellent agreement with the radiative power measured from high-energy γ rays (see Section 7, particularly Figure 9, right panel). This approach seems to be not suitable for 15 GHz data, as radio observations at this frequency are sampling the jet downstream, where the flux variability is affected by effects other than radiative losses only [26].
- The use of single-dish flux densities at 37 GHz (Section 5), with k_2 calculated from 15 and 43 GHz observations (see Equation (9)), is consistent with the power derived from VLBA observations. The best result is with 43 GHz data, as expected, because of the smaller difference in frequency.
- The kinetic power calculated on the basis of the extended radio emission at MHz frequencies and the relationships by [35,36] (Section 6) gives better results when compared with the power estimated from the Blandford and Königl [27] model and 15 GHz data. However, we noted a systematic disagreement of the power for weak sources ($P_{kin} \lesssim 10^{44}$ erg/s).
- The comparison of the radiative power estimated from the Blandford and Königl [27] model and high-energy γ-ray observations from *Fermi*/LAT (Section 7) resulted in an excellent agreement, particularly with 43 GHz data, and when taking into account the Compton dominance. The larger dispersion in the comparison with 15 GHz data seems to be due to the above-cited limitations of δ calculated via T_b (Figure 10). However, a

quite good agreement with 15 GHz data is recovered when using a constant value for Γ^2/δ^4 to estimate the radiative power, even though it is systematically lower than the value from radio observations and is likely to be a chance coincidence (Section 8).
- Searching for an easy-to-use equation to estimate the jet power, we proposed Equation (27), based on the limited range of values of k_2, particularly from 15 GHz data. The comparison of power derived from 15, 37, and 43 GHz data is fairly correlated ($\rho \sim 0.9$) with an acceptable dispersion $\sigma \sim 0.4$. The use of a constant Γ^2/δ^4 to estimate the radiative power from the γ-ray luminosity resulted in a slightly greater dispersion ($\sigma \sim 0.6$–0.7).

For the sake of simplicity, we recall in Table 6 the proposed easy-to-use equations to estimate the jet power, with the caveat of divergence at low and high powers.

Table 6. Jet power in [erg s^{-1}] calculated with our proposed easy-to-use equations based on fudge factors described in Section 8. We remind that the radio flux density S_ν is measured in [Jy], the luminosity distance $d_{L,9}$ is in [Gpc], and L_γ is in [erg s^{-1}].

Jet Power	Equation	Notes
Total	$(4.5 \times 10^{44}) \left(\frac{S_\nu d_{L,9}^2}{1+z} \right)^{\frac{12}{17}}$	From Equation (11)
Kinetic	$(3.9 \times 10^{44}) \left(\frac{S_\nu d_{L,9}^2}{1+z} \right)^{\frac{12}{17}}$	From Equation (13)
Radiative (synchrotron)	$(5.6 \times 10^{43}) \left(\frac{S_\nu d_{L,9}^2}{1+z} \right)^{\frac{12}{17}}$	From Equation (12)
Radiative (Compton)	$0.0027 L_\gamma$	From Equation (23)

We want to stress that equations in Table 6 must be used with great care because the fudge factors are affected by the variability of the source and the uncertainties in the measurement or derivation of the physical quantities $\beta, \Gamma, \delta, \theta$, and ϕ (that we did not consider in this work). However, given the difficulty of measuring or inferring all these quantities without dedicated VLBA observations (preferably at high frequencies, such as 43 GHz), these equations can offer a useful first estimate of the jet power, being careful when dealing with extremely weak or extremely powerful jets.

Before concluding, some more words of caveat should be written, which are also the points to be addressed to improve our methods to estimate the jet power. The possible sources of bias in the present work are as follows:

- The sample is composed mostly of blazars (30/32 objects), whose electromagnetic emission is dominated by relativistic beaming, because of the small viewing angle. Only two objects are misaligned AGN (radio galaxies), and there are no jetted Seyferts. It is necessary to expand the sample to cover all types of jetted AGN, beamed or not.
- To convert redshifts into luminosity distances, we employed the simplified Equation (1). This resulted in an overestimation of the luminosity distance of $\sim$10% for the farthest object (J0841 + 7053, $z = 2.71$), which quickly decreases to $\sim$4% for objects at $z \sim 1$. This is not a problem in the present work, since we compared the jet power of the same object calculated with different methods, but a comparison with values from other works should be dealt with care in the case of high-redshift objects.
- The Blandford and Königl [27] model is for flat-spectrum radio sources. Deviation from a flat radio spectrum, such as in cases of steep spectra of misaligned AGN, might imply large errors. In our sample, we have only two radio galaxies, too few to draw useful conclusions.
- The extended radio emission to estimate the kinetic power (Section 6) should be only due to radio lobes, with a steep spectrum. However, for the sake of simplicity, we considered the whole integrated flux. As a matter of fact, the typical resolution at 200–400 MHz is about one arcminute, which is equivalent to $\sim$0.1 Mpc at $z \sim 0.1$. Therefore, most of the objects in our sample are pointlike at MHz fre-

quencies, and it is not possible to isolate the steep-spectrum extended emission from the core. Anyway, at MHz frequencies, the core contribution should be less important than the lobes. The low-frequency array (LOFAR) might be a viable solution for a better angular resolution ($\sim 0.21''$ at 240 MHz for a 1000 km baseline (https://science.astron.nl/telescopes/lofar/lofar-system-overview/observing-modes/lofar-imaging-capabilities-and-sensitivity/, accessed on 27 March 2024)), but it is necessary to recalibrate Equations (20) and (21) because the maximum frequency of LOFAR is 250 MHz.

- In this work, we always used median or weighted mean values calculated over long periods. The shortest period is 2007–2013, about 5.5 years. Given the strong variability of jetted AGN, the use of values from single-epoch observations or from only one VLBA knot might result in significant deviations. For example, we considered J0433 + 0521 with VLBA data at 43 GHz: the total jet power with the data used in this work results to be $\sim 2.1 \times 10^{44}$ erg/s. We want to compare with the most recent data from [44], which extended the work in [11] to December 2018. By using the median values, we calculate $\sim 4.1 \times 10^{44}$ erg/s, consistent within a factor 2 with the present work. If we calculate the jet power by using the data, for example, of the component C15 only, we obtain $\sim 5.2 \times 10^{43}$ erg/s, about one order of magnitude smaller.
- We also need to underline that this work was conducted by considering the same physical factors $\Delta = \log(r_{\rm max}/r_{\rm min})$ and $\Lambda = \log(\gamma_{\rm e,max}/\gamma_{\rm e,min})$ for all the sources. Therefore, a part of the dispersions in the comparisons is surely due to this assumption. For example, an outburst changing the electron distribution will alter Λ, which in turn will change the coefficient k_1 of Equation (8). Therefore, it is necessary to also address the microphysics of the jet and, particularly, the particle content (leptons vs. hadrons), the energy distribution of electrons, the size of the emission region vs. opacity, and the equipartition hypothesis.

Author Contributions: Conceptualization, L.F.; writing—original draft, L.F.; writing—review and editing, L.F., B.D.B., M.T., H.A., P.M., A.P.M., S.G.J., E.J., S.A. and E.D.B. All authors have read and agreed to the published version of the manuscript.

Funding: This research received no external funding.

Data Availability Statement: This research made use of publicly available data from the VLBA Boston University blazar program [11,21], the MOJAVE program [25], the Metsähovi Radio Observatory (https://www.metsahovi.fi/opendata/, accessed on 27 March 2024), the CATS database [37], and the *Fermi* LAT Light Curve Repository [39]. Recalculated or new values resulting from this work are available upon reasonable requests.

Acknowledgments: L.F. would like to thank (in alphabetical order) Stefano Ciroi, Maria J. M. Marchã, Patrizia Romano, and Stefano Vercellone for their valuable comments on the draft.

Conflicts of Interest: The authors declare no conflicts of interest.

References

1. Blandford, R.; Meier, D.; Readhead, A. Relativistic Jets from Active Galactic Nuclei. *Annu. Rev. Astron. Astrophys.* **2019**, *57*, 467–509. [CrossRef]
2. Foschini, L. Some notes about the current researches on the physics of relativistic jets. *Front. Astron. Space Sci.* **2022**, *8*, 794891. [CrossRef]
3. Pjanka, P.; Zdziarski, A.A.; Sikora, M. The power and production efficiency of blazar jets. *Mon. Not. R. Astron. Soc.* **2017**, *465*, 3506–3514. [CrossRef]
4. Ghisellini, G.; Tavecchio, F. Canonical high-power blazars. *Mon. Not. R. Astron. Soc.* **2009**, *397*, 985–1002. [CrossRef]
5. Ghisellini, G.; Tavecchio, F.; Maraschi, L.; Celotti, A.; Sbarrato, T. The power of relativistic jets is larger than the luminosity of their accretion disks. *Nature* **2014**, *515*, 376–378. [CrossRef] [PubMed]
6. Lobanov, A. Ultracompact jets in active galactic nuclei. *Astron. Astrophys.* **1998**, *330*, 79–89.
7. Zdziarski, A.A.; Sikora, M.; Pjanka, P.; Tchekhovskoy, A. Core shifts, magnetic field and magnetization of extragalactic jets. *MNRAS* **2015**, *451*, 927–935. [CrossRef]

8. Willot, C.J.; Rawlings, S.; Blundell, K.M.; Lacy, M. The emission line-radio correlation for radio sources using the 7C redshift survey. *Mon. Not. R. Astron. Soc.* **1999**, *309* 1017–1033. [CrossRef]
9. Nemmen, R.S.; Georganopoulos, M.; Guiriec, S.; Meyer, E.T.; Gehrels, N.; Sambruna, R.M. A Universal Scaling for the Energetics of Relativistic Jets from Black Hole Systems. *Science* **2012**, *338*, 1445–1448. [CrossRef]
10. Foschini, L.; Lister, M.; Hovatta, T.; Kovalev, Y.; Romano, P.; Vercellone, S.; Lähteenmäki, A.; Savolainen, T.; Tornikoski, M.; Angelakis, E.; et al. Calibrating The Power Of Relativistic Jets. In Proceedings of the High Energy Phenomena in Relativistic Outflows VII ((HEPRO VII)), Barcelona, Spain, 9–12 July 2019; Volume 354.
11. Jorstad, S.G.; Marscher, A.P.; Morozova, D.A.; Troitsky, I.S.; Agudo, I.; Casadio, C.; Foord, A.; Gómez, J.L.; MacDonald, N.R.; Molina, S.N.; et al. Kinematics of parsec-scale jets of gamma-ray blazars at 43 GHz within the VLBA-BU-BLAZAR program. *Astrophys. J.* **2017**, *846*, 98. [CrossRef]
12. Pushkarev, A.B.; Kovalev, Y.Y.; Lister, M.L.; Savolainen, T. MOJAVE—XIV. Shapes and opening angles of AGN jets. *Mon. Not. R. Astron. Soc.* **2017**, *468*, 4992–5003. [CrossRef]
13. Liodakis, I.; Hovatta, T.; Huppenkothen, D.; Kiehlmann, S.; Max-Moerbeck, W.; Readhead, A.C.S. Constraining the Limiting Brightness Temperature and Doppler Factors for the Largest Sample of Radio-bright Blazars. *Astrophys. J.* **2018**, *866*, 137. [CrossRef]
14. Finke, J.D. The properties of parsec-scale blazar jets. *Astrophys. J.* **2019**, *870*, 28. [CrossRef]
15. Paliya, V.S.; Marcotulli, L.; Ajello, M.; Joshi, M.; Sahayanathan, S.; Rao, A.R.; Hartmann, D. General Physical Properties of CGRaBS Blazars. *Astrophys. J.* **2017**, *851*, 33. [CrossRef]
16. Paliya, V.S.; Parker, M.L.; Jiang, J.; Fabian, A.C.; Brenneman, L.; Ajello, M.; Hartmann, D. General Physical Properties of Gamma-Ray-emitting Narrow-line Seyfert 1 Galaxies. *Astrophys. J.* **2019**, *872*, 169. [CrossRef]
17. Meyer, E.T.; Fossati, G.; Georganopoulos, M.; Lister, M.L. From the Blazar Sequence to the Blazar Envelope: Revisiting the Relativistic Jet Dichotomy in Radio-loud Active Galactic Nuclei. *Astrophys. J.* **2011**, *740*, 98. [CrossRef]
18. Nokhrina, E.E.; Beskin, V.S.; Kovalev, Y.Y.; Zheltoukhov, A.A. Intrinsic physical conditions and structure of relativistic jets in active galactic nuclei. *Mon. Not. R. Astron. Soc.* **2015**, *447*, 2726–2737. [CrossRef]
19. Foschini, L. The Unification of Relativistic Jets. *Int. J. Mod. Phys. Conf. Ser.* **2014**, *28*, 1460188. [CrossRef]
20. Riess, A.G.; Yuan, W.; Macri, L.M.; Scolnic, D.; Brout, D.; Casertano, S.; Jones, D.O.; Murakami, Y.; Anand, G.S.; Breuval, L.; et al. A Comprehensive Measurement of the Local Value of the Hubble Constant with 1 km s^{-1} Mpc^{-1} Uncertainty from the Hubble Space Telescope and the SH0ES Team. *Astrophys. J.* **2022**, *934*, L7. [CrossRef]
21. Jorstad, S.; Marscher, A. The VLBA-BU-BLAZAR Multi-Wavelength Monitoring Program. *Galaxies* **2016**, *4*, 47. [CrossRef]
22. Foschini, L.; Lister, M.L.; Andernach, H.; Ciroi, S.; Marziani, P.; Antón, S.; Berton, M.; Dalla Bontà, E.; Järvelä, E.; Marchã, M.J.M.; et al. A New Sample of Gamma-Ray Emitting Jetted Active Galactic Nuclei. *Universe* **2022**, *8*, 587. [CrossRef]
23. Matt, G.; Guainazzi, M.; Maiolino, R. Changing look: From Compton-thick to Compton-thin, or the rebirth of fossil active galactic nuclei. *Mon. Not. R. Astron. Soc.* **2003**, *342*, 422–426. [CrossRef]
24. Ricci, C.; Trakhtenbrot, B. Changing-look Active Galactic Nuclei. *arXiv* **2022**, arXiv:2211.05132.
25. Lister, M.L.; Aller, M.F.; Aller, H.D.; Hodge, M.A.; Homan, D.C.; Kovalev, Y.Y.; Pushkarev, A.B.; Savolainen, T. MOJAVE XV. VLBA 15 GHz Total Intensity and Polarization Maps of 437 Parsec-scale AGN Jets from 1996 to 2017. *Astrophys. J. Suppl. Ser.* **2018**, *234*, 12. [CrossRef]
26. Homan, D.C.; Cohen, M.H.; Hovatta, T.; Kellermann, K.I.; Kovalev, Y.Y.; Lister, M.L.; Popkov, A.V.; Pushkarev, A.B.; Ros, E.; Savolainen, T. MOJAVE XIX. Brightness Temperatures and Intrinsic Properties of Blazar Jets. *Astrophys. J.* **2021**, *923*, 67. [CrossRef]
27. Blandford, R.D.; Königl, A. Relativistic Jets as Compact Radio Sources. *Astrophys. J.* **1979**, *232*, 34–48. [CrossRef]
28. Clausen-Brown, E.; Savolainen, T.; Pushkarev, A.B.; Kovalev, Y.Y.; Zensus, J.A. Causal connection in parsec-scale relativistic jets: results from the MOJAVE VLBI survey. *Astron. Astrophys.* **2013**, *558*, A144. [CrossRef]
29. Readhead, A.C.S. Equipartition Brightness Temperature and the Inverse Compton Catastrophe. *Astrophys. J.* **1994**, *426*, 51–59. [CrossRef]
30. Edwards, P.G.; Piner, B.G. The Subluminal Parsec-Scale Jet of Markarian 501. *Astrophys. J.* **2002**, *579*, L67–L70. [CrossRef]
31. Piner, B.G.; Edwards, P.G. The Parsec-Scale Structure and Jet Motions of the TeV Blazars 1ES 1959 + 650, PKS 2155 − 304, and 1ES 2344 + 514. *Astrophys. J.* **2004**, *600*, 115–126. [CrossRef]
32. Hovatta, T.; Valtaoja, E.; Tornikoski, M.; Lähteenmäki, A. Doppler factors, Lorentz factors, and viewing angles for quasars, BL Lacertae objects and radio galaxies. *Astron. Astrophys.* **2009**, *494*, 527–537. [CrossRef]
33. Teräsranta, H.; Tornikoski, M.; Mujunen, A.; Karlamaa, K.; Valtonen, T.; Henelius, N.; Urpo, S.; Lainela, M.; Pursimo, T.; Nilsson, K.; et al. Fifteen years monitoring of extragalactic radio sources at 22, 37 and 87 GHz. *Astron. Astrophys. Suppl.* **1998**, *132*, 305–331. [CrossRef]
34. McNamara, B.R.; Wise, M.; Nulsen, P.E.J.; David, L.P.; Sarazin, C.L.; Bautz, M.; Markevitch, M.; Vikhlinin, A.; Forman, W. R.; Jones, C.; et al. Chandra X-ray Observations of the Hydra A Cluster: An Interaction between the Radio Source and the X-ray-emitting Gas. *Astrophys. J.* **2000**, *534*, L135-L138. [CrossRef] [PubMed]
35. Bîrzan, L.; McNamara, B.R.; Nulsen, P.E.J.; Carilli, C.L.; Wise, M.W. Radiative efficiency and content of extragalactic radio sources: Toward a universal scaling relation between jet power and radio power. *Astrophys. J.* **2008**, *686*, 859–880. [CrossRef]
36. Cavagnolo, K.W.; McNamara, B.R.; Nulsen, P.E.J.; Carilli, C.L.; Jones, C.; Bîrzan, L. A relationship between AGN jet power and radio power. *Astrophys. J.* **2010**, *720*, 1066–1072. [CrossRef]

37. Verkhodanov, O.V.; Trushkin, S.A.; Andernach, H.; Chernenkov, V.N. Current status of the CATS database. *arXiv* **2005**, arXiv:0705.2959.
38. Atwood, W.B. et al. [Fermi LAT Collaboration]. The Large Area Telescope on the Fermi Gamma-Ray Space Telescope Mission. *Astrophys. J.* **2009**, *697*, 1071–1102. [CrossRef]
39. Abdollahi, S. et al. [Fermi LAT Collaboration]. The Fermi-LAT Lightcurve Repository. *Astrophys. J. Suppl.* **2023**, *265*, 31. [CrossRef]
40. Maraschi, L.; Tavecchio, F. The jet-disk connection and blazar unification. *Astrophys. J.* **2003**, *593*, 667–675. [CrossRef]
41. Böttcher, M.; Harris, D.E.; Krawczynski, H. (Eds.) *Relativistic Jets from Active Galactic Nuclei*; Wiley: Weinheim, Germany, 2012.
42. Ghisellini, G.; Tavecchio, F.; Foschini, L.; Ghirlanda, G.; Maraschi, L.; Celotti, A. General physical properties of bright Fermi blazars. *Mon. Not. R. Astron. Soc.* **2010**, *402*, 497–518. [CrossRef]
43. Jorstad, S.G.; Marscher, A.P.; Lister, M.L.; Stirling, A.M.; Cawthorne, T.V.; Gear, W.K.; Gómez, J.L.; Stevens, J.A.; Smith, P.S.; Forster, J.R.; et al. Polarimetric Observations of 15 Active Galactic Nuclei at High Frequencies: Jet Kinematics from Bimonthly Monitoring with the Very Long Baseline Array. *Astron. J.* **2005**, *130*, 1418–1465. [CrossRef]
44. Weaver, Z.R.; Jorstad, S.G.; Marscher, A.P.; Morozova, D.A.; Troitsky, I.S.; Agudo, I.; Gómez, J.L.; Lähteenmäki, A.; Tammi, J.; Tornikoski, M. Kinematics of Parsec-scale Jets of Gamma-Ray Blazars at 43 GHz during 10 yr of the VLBA-BU-BLAZAR Program. *Astrophys. J. Suppl. Ser.* **2022**, *260*, 12. [CrossRef]